ELSEVIER

International Journal of Solids and Structures 41 (2004) 5517–5540

INTERNATIONAL JOURNAL OF SOLIDS and STRUCTURES

www.elsevier.com/locate/ijsolstr

Geometric design of arbitrarily curved bi-stable deployable arches with discrete joint size

C.J. Gantes *, E. Konitopoulou

Metal Structures Laboratory, National Technical University of Athens, Greece, P.O. Box 31830, GR-10035 Athens, Greece

Received 12 April 2004; received in revised form 12 April 2004
Available online 7 June 2004

Abstract

The deployable structures presented in this work are bi-stable in the sense of being self-standing and stress-free when fully closed or fully deployed, but exhibit incompatibilities between the member lengths at intermediate geometric configurations during the deployment process, which lead to the occurrence of second-order strains and stresses resulting in a snap-through phenomenon that "locks" the structures in their deployed configuration. Until now the geometric shapes that were possible in the deployed configuration were only flat or curved with constant curvature. This limitation is addressed in the present paper by proposing a geometric design methodology for deployable arches of arbitrary curvature, accounting also for the discrete joint size, and applying it successfully for the geometric design of a semi-elliptical arch. The arch is then modeled with finite elements, and a geometrically non-linear analysis is performed in order to verify the deployability feature. Further verification is provided by the construction of a small-scale physical model. A preliminary structural design indicates the overall feasibility of the arch for short to medium spans and light loads.

Keywords: Deployable structures; Snap-through; Geometric design; Arbitrary curvature; Discrete joint size; Semi-elliptical arch; Geometrically non-linear finite element analysis; Physical model; Preliminary structural design

1. Introduction

Deployable structures are prefabricated space frames consisting of straight bars linked together in the factory as a compact bundle, which can then be unfolded into large-span, load bearing structural shapes by simple articulation. Because of this feature they offer significant advantages in comparison to conventional, non-deployable structures for a wide spectrum of applications ranging from temporary structures to the aerospace industry, being mainly characterized by their feature of transforming and adapting to changing needs.

* Corresponding author. Tel.: +30-210-7723440; fax: +30-210-7723442.
E-mail address: chgantes@central.ntua.gr (C.J. Gantes).

0020-7683/$ - see front matter © 2004 Elsevier Ltd. All rights reserved.
doi:10.1016/j.ijsolstr.2004.04.030

Because of their numerous advantages, deployable structures have been investigated, designed and constructed by many engineers both for earth and space applications (Pinero, 1962; Zeigler, 1984; Rhodes, 1984; Merchan, 1987; Miura and Furuya, 1988; Escrig et al., 1989; Kwan and Pellegrino, 1991; Kuznetsov, 1991; You and Pellegrino, 1993; Pellegrino and Guest, 2000; You, 2000; Escrig and Brebbia, 2000; Furuya and Kawasaki, 2000; Kawaguchi and Kondo, 2000; Langbecker and Albermani, 2001). The concept as well as the geometric and structural characteristics of the type of deployable structures considered here are the product of research work carried out since 1985 at the Massachusetts Institute of Technology, the Technion in Israel and the National Technical University of Athens (Gantes, 1991; Gantes et al., 1991; Gantes et al., 1994a; Gantes, 2000a), that succeeded in converting the primary ideas that were suggested earlier (Krishnapillai and Zalewski, 1985) to a feasible type of structure. The main findings of this work are included in a recent book (Gantes, 2001).

A fundamental design requirement of the structures investigated here is that they have two states in which they are self-standing and stress-free, namely when they are fully closed or fully deployed, hence they can be called bi-stable. However, at intermediate geometric configurations during the deployment process incompatibilities between the member lengths lead to the occurrence of second-order strains and stresses resulting in a snap-through phenomenon that "locks" the structure in its deployed configuration. The structural response during deployment is, hence, characterized by geometric non-linearities, and simulation of the deployment process is, therefore, a very important problem requiring sophisticated finite element modeling (Gantes, 2000a). The material behavior, however, must remain linearly elastic, so that no residual stresses reduce the load bearing capacity under service loads (Gantes, 1996).

From a structural point of view, deployable structures have to be designed for two completely different loading conditions, under service loads in the deployed configuration, and during deployment. The structural design process is very complicated and requires successive iterations to achieve some balance between desired flexibility during deployment and desired stiffness in the deployed configuration (Gantes et al., 1993a,b, 1994b; Gantes, 1997).

From a geometric point of view, the whole idea of this type of deployable structures is based on the so-called scissor-like elements (SLEs), pairs of bars connected to each other at an intermediate point through a pivotal connection which allows them to rotate freely about an axis perpendicular to their common plane but restrains all other degrees of freedom, while, at the same time, their end points are hinged to the end points of other SLEs. Several SLEs are connected to each other in order to form units with regular polygonal plan views, for example triangular, square, or hexagonal units like the ones shown in Fig. 1. The sides and radii of the polygons are SLEs. These polygons, in turn, are linked in appropriate arrangements constituting deployable structures, which are either flat or curved in their final deployed configuration (Fig. 2).

Geometric design is performed according to a set of geometric constraints resulting from the requirement of zero stresses at the two extreme configurations (Gantes, 1993; Gantes et al., 1993c,d, 1997). Stress-free implies undeformed; therefore, the straightness of the bars in the deployed configuration is the starting point for geometric design. Several constraint equations emanate from this condition. The way to derive these equations is by looking at the development of adjacent scissor-like elements on a common plane and applying basic geometric and trigonometric rules. The additional functional requirement that has to be satisfied through geometric design is a stress-free state in the folded configuration. By translating this also into a demand for straightness, one can obtain the so-called deployability constraint (Fig. 3), which requires that the sums of the lengths between pivot and end node of the bars of SLEs that are connected to each other are equal.

The geometric constraint equations are derived by applying the above rules for all scissor-like elements of a unit, taking also symmetry or other special conditions into account. The formulation of a design procedure based on these constraint equations must be preceded by the choice of design parameters. Such parameters are usually some external dimensions of the units, which are often imposed by architectural

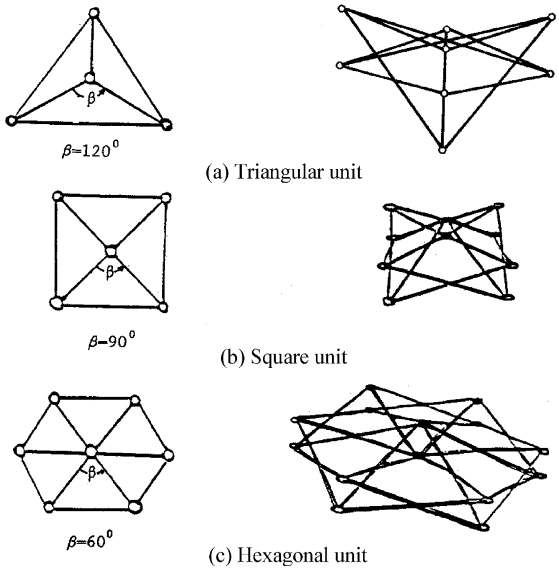

Fig. 1. Plan views (left) and perspective views (right) of typical polygonal deployable units.

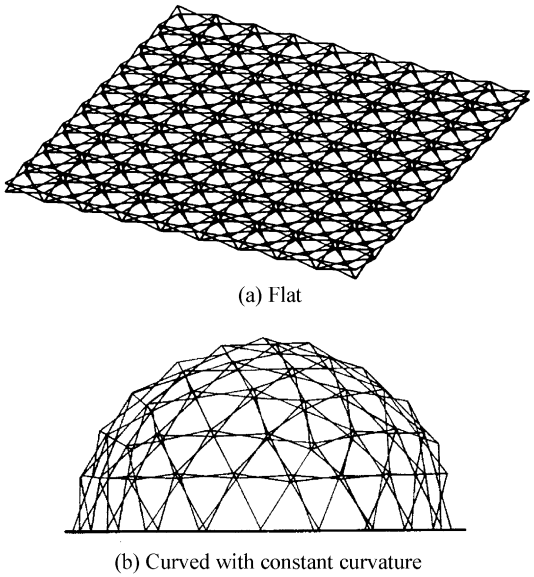

Fig. 2. Deployable structures in their deployed configuration.

requirements. The other quantities that define the geometry, such as member lengths or angles between the members in the deployed configuration, are the unknown variables. Following this approach, one ends up with a system of simultaneous non-linear equations that have to be solved numerically using an iterative algorithm such as the Newton–Raphson method.

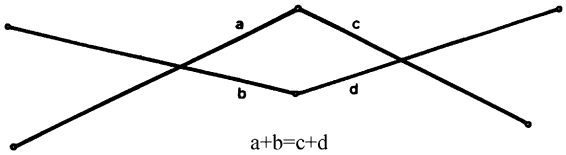

Fig. 3. Deployability constraint.

This geometric design approach is initially followed at a polygonal unit level. Then, the additional constraints for deployment compatibility between adjacent units, and how this affects the overall geometric design process, must be accounted for. However, the snap-through-type deployable structures that had been designed so far according to this approach suffered from a significant limitation. The geometric shapes that were possible in the deployed configuration were only flat or curved with constant curvature (Fig. 2). Other shapes, which might be structurally more efficient or architecturally more desirable, could not be achieved by using these units.

In the present paper this limitation is addressed by unifying the two stages of the approach, namely design of individual units and then connectivity between adjacent units, into one (Konitopoulou, 2001; Gantes and Konitopoulou, 2002). Thus, the desired final shape of the deployed structure is taken into account during geometric design of individual units. This increases the order of the resulting system of simultaneous equations, and thus the computational effort, but seems to be the only way to design snap-through-type deployable structures of arbitrary curvature. In addition, individual polygons are no longer necessarily regular and identical to each other.

The geometric constraints according to this approach, proposed earlier by Konitopoulou (2001) and Gantes and Konitopoulou (2002), are extended here in order to take the discrete joint size into account. The steps of a corresponding systematic geometric design methodology are listed in detail. This methodology is applied successfully for the geometric design of a semi-elliptical arch. A small-scale physical model of the arch is constructed in order to demonstrate the correctness of the proposed approach. The arch is then modeled with finite elements, and a geometrically non-linear analysis is performed in order to verify the deployability feature. Extension of the methodology to other geometric shapes does not appear to present any additional conceptual difficulties.

2. Geometric constraints for elliptical deployable arch

The proposed approach is applicable for the geometric design of any arch whose axis is described by an equation of the type:

$$f(x,y)=0 \tag{1}$$

For the sake of clarity and without loss of generality, the approach will be demonstrated for the case of a semi-elliptical arch. Consider an ellipse that will be the axis of the arch, shown in Fig. 4 and described by the equation:

$$\frac{x^2}{a^2}+\frac{y^2}{b^2}=1 \tag{2}$$

Furthermore, consider two more ellipses, having the same axes lengths a, b as the previous one, that are placed on both sides of the original one (Fig. 5) at a specific distance that will be defined later on. Thus, the upper surface of the elliptical arch is created. Then, this surface is divided into consecutive segments, having the same arch length (Fig. 6). Because of the elliptical shape, the chords of the respective arch segments are

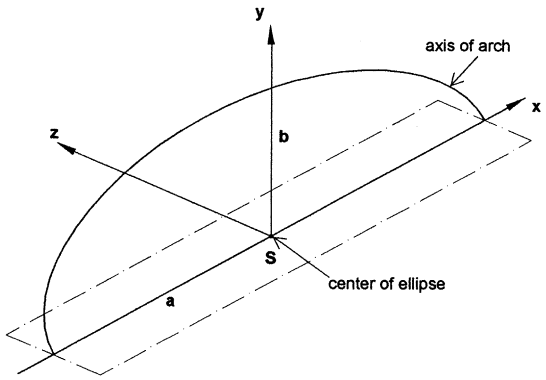

Fig. 4. Axis of elliptical arch.

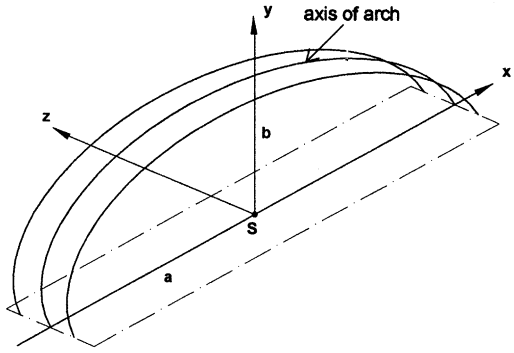

Fig. 5. Upper surface of elliptical arch.

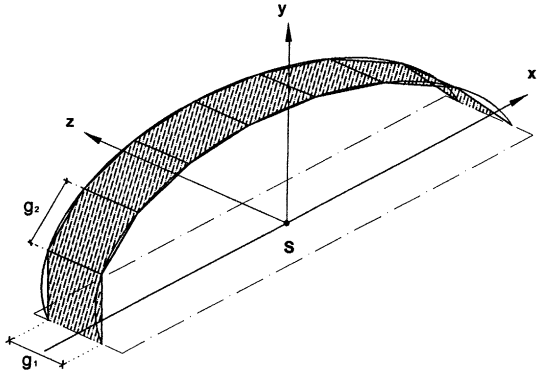

Fig. 6. Sub-division of upper surface of elliptical arch in sub-planes.

of different length, called g_2. The distance g_1 between the ellipses placed on both sides of the axis is defined as equal to the average of all g_2. With the subdivision of the upper elliptical surface, an inscribed convex polyhedron is created. Each sub-plane will constitute the top view of a single structural deployable unit.

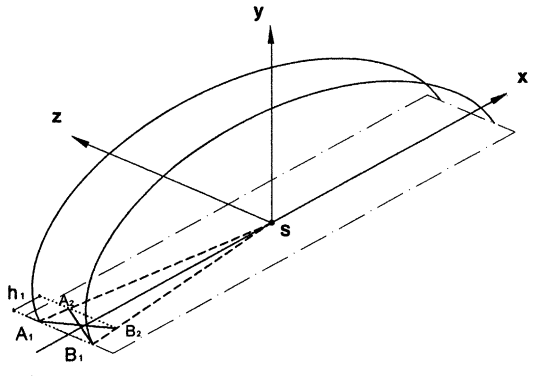

Fig. 7. Location of first SLE.

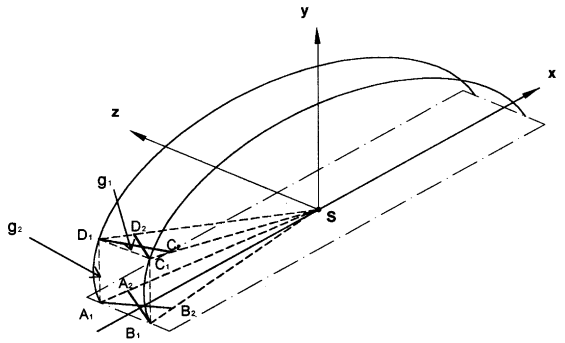

Fig. 8. Location of second SLE.

Thus, the geometric design of the elliptical arch begins with the first structural unit. Some geometric parameters, such as the total span of the arch and the size of the individual unit are known, because they are imposed by architectural requirements. Assuming that the dimensions of the elliptical surface are known, the coordinates of points A_1 and B_1 (Fig. 7), defined as the intersection of the two ellipses with the xz plane, can be chosen.

If S is the center of the ellipse, then the points A_2 and B_2 belong to lines SA_1 and SB_1 and are at distance h_1 from A_1 and B_1, respectively, where h_1 is the thickness of the structural unit (Fig. 7). Points C_1 and D_1 are on the elliptical surface and more specifically on the two edge ellipses. Their distance from B_1 and A_1, respectively, is g_2 (Fig. 8). Similarly, points C_2 and D_2 are at distance h_2 from C_1 and D_1, respectively. The point O_1, which is the peak of the polygonal unit, is on the axis of the elliptical arch and more specifically in the middle of the unit's arch segment (Fig. 9). The same holds for point O_2, and the distance between O_1 and O_2 is h_3. The dimensions h_2 and h_3 are not design parameters, but are derived from the solution of the geometric design problem for the structural unit. Thus, the solution of the structural unit starts with the coordinates of points A_1, A_2, B_1, B_2, C_1, D_1, O_1 and S as known parameters. The coordinates of points C_2, D_2, and O_2 are unknown. The complete first structural unit is shown in Fig. 10.

2.1. Geometric constraints assuming idealized joints

For the geometric design of the elliptical arch several different types of SLEs are used, contrary to the case of curved structures with constant curvature. In particular, the outer planes of the unit $A_1A_2B_1B_2$ and

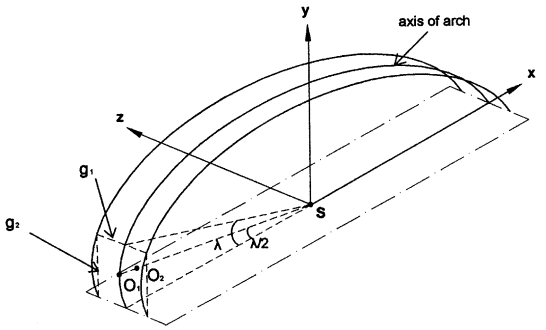

Fig. 9. Location of points O_1 and O_2.

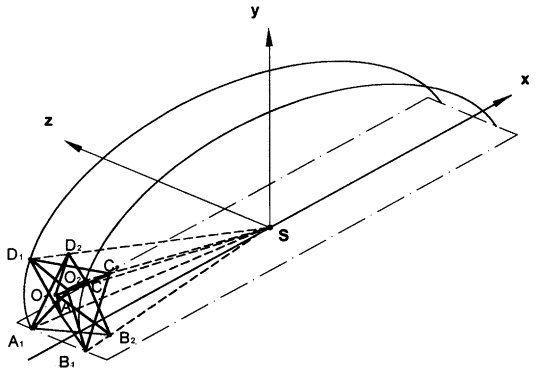

Fig. 10. First basic square unit.

$C_1C_2D_1D_2$ are determined by symmetrical but different to each other SLEs, while the planes $A_1A_2D_1D_2$ and $B_1B_2C_1C_2$ are defined by non-symmetrical SLEs, which are the same for both of them (Fig. 11). Similarly, the inner planes $O_1O_2A_1A_2$, $O_1O_2B_1B_2$, $O_1O_2C_1C_2$ and $O_1O_2D_1D_2$ are illustrated in Fig. 12. Assuming that all the above are known, the angles φ_1, φ_2, φ_3, ω_1, ω_2, ψ_1, ψ_2, ψ_3, ψ_4, ψ_5, ψ_6 and the lengths L_1, L_2, which are defined in Figs. 11 and 12, can be derived. L_1 and L_2 are found as the distances between two points with known coordinates, for example:

$$L_1 = \sqrt{(x_{O1} - x_{A1})^2 + (y_{O1} - y_{A1})^2 + (z_{O1} - z_{A1})^2} \tag{3}$$

For the angles the cosines law is used. For example angle φ_1 is obtained from the equation:

$$(A_1B_1)^2 = (A_1S)^2 + (B_1S)^2 - 2(A_1S)(B_1S)\cos\varphi_1 \tag{4}$$

In order to derive the geometric constraints for the units, let us consider the development of two SLEs on a common plane. Two of them are shown indicatively in Fig. 13. The following equations can be written for this problem:

Foldabillity constraints:

- Between outer SLEs:

$$e_1 + f_1 = e_3 + f_3, \qquad e_2 + f_2 = e_4 + f_4 \tag{5}$$

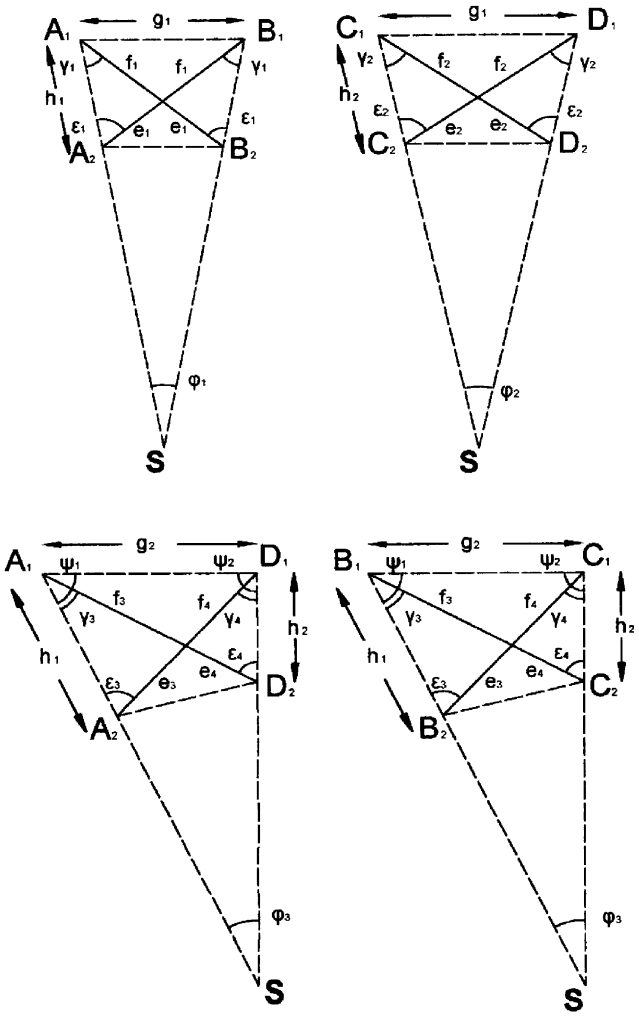

Fig. 11. Outer SLEs.

- Between inner SLEs:

$$a_1 + b_1 = a_2 + b_2 \tag{6}$$

- Between inner and outer SLEs:

$$e_1 + f_1 = c_1 + d_1, \qquad e_2 + f_2 = c_2 + d_2 \tag{7}$$

Sines law:

- For the outer SLEs:

$$\frac{e_1}{f_1} = \frac{\sin\gamma_1}{\sin\varepsilon_1}, \qquad \frac{e_2}{f_2} = \frac{\sin\gamma_2}{\sin\varepsilon_2}, \qquad \frac{e_3}{f_3} = \frac{\sin\gamma_3}{\sin\varepsilon_3}, \qquad \frac{e_4}{f_4} = \frac{\sin\gamma_4}{\sin\varepsilon_4} \tag{8}$$

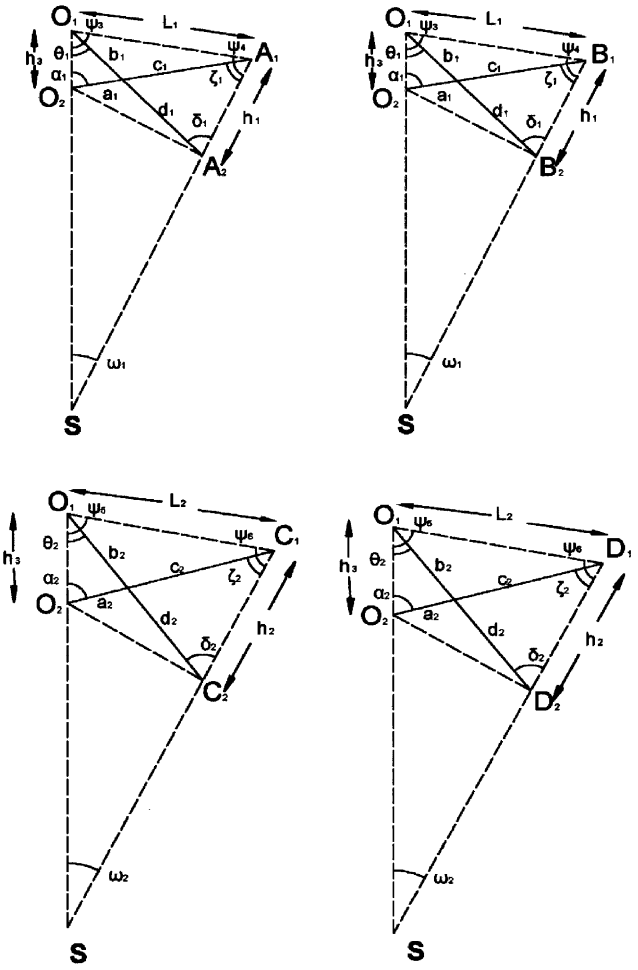

Fig. 12. Inner SLEs.

- For the inner SLEs:

$$\frac{a_1}{b_1}=\frac{\sin\theta_1}{\sin\alpha_1},\qquad \frac{c_1}{d_1}=\frac{\sin\delta_1}{\sin\zeta_1},\qquad \frac{a_2}{b_2}=\frac{\sin\theta_2}{\sin\alpha_2},\qquad \frac{c_2}{d_2}=\frac{\sin\delta_2}{\sin\zeta_2} \tag{9}$$

Length projections in the radial direction:

- For the outer SLEs:

$$\begin{aligned} &e_1\cos\varepsilon_1+f_1\cos\gamma_1=h_1, \qquad e_2\cos\varepsilon_2+f_2\cos\gamma_2=h_2\\ &e_3\cos\varepsilon_3+f_3\cos\gamma_3=h_1, \qquad e_4\cos\varepsilon_4+f_4\cos\gamma_4=h_2 \end{aligned} \tag{10}$$

- For the inner SLEs:

$$\begin{aligned} &a_1\cos\alpha_1+b_1\cos\theta_1=h_3, \qquad c_1\cos\zeta_1+d_1\cos\delta_1=h_1\\ &a_2\cos\alpha_2+b_2\cos\theta_2=h_3, \qquad c_2\cos\zeta_2+d_2\cos\delta_2=h_2 \end{aligned} \tag{11}$$

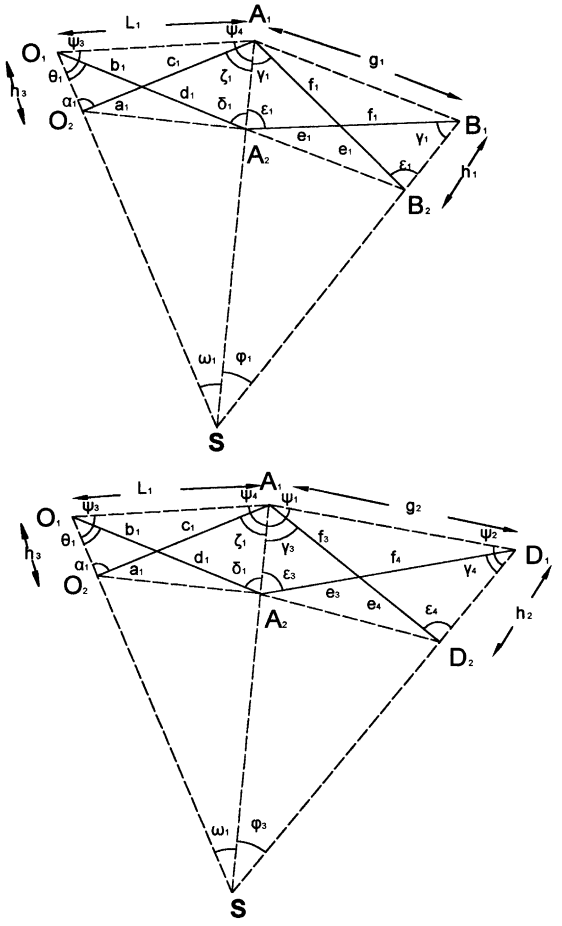

Fig. 13. Adjacent outer and inner SLEs.

Length projections in the tangential direction:

- For the outer SLEs:

$$2f_1 \sin\left(\frac{\varepsilon_1+\gamma_1}{2}\right) = g_1, \qquad 2f_2 \sin\left(\frac{\varepsilon_2+\gamma_2}{2}\right) = g_1, \qquad f_3\cos(\psi_1-\gamma_3) + f_4\cos(\psi_2-\gamma_4) = g_2 \tag{12}$$

- For the inner SLEs:

$$b_1\cos(\psi_3-\theta_1) + c_1\cos(\psi_4-\zeta_1) = L_1, \qquad b_2\cos(\psi_5-\theta_2) + c_2\cos(\psi_6-\zeta_2) = L_2 \tag{13}$$

Concurrency of lines O_1O_2, A_1A_2, B_1B_2:

$$\begin{aligned} &\varepsilon_3+\gamma_3 = \varepsilon_4+\gamma_4, \qquad \alpha_1+\theta_1 = \delta_1+\zeta_1, \qquad \alpha_2+\theta_2 = \delta_2+\zeta_2, \qquad \gamma_1+\varphi_1 = \varepsilon_1 \\ &\gamma_2+\varphi_2 = \varepsilon_2, \qquad \gamma_4+\varphi_3 = \varepsilon_3, \qquad \zeta_1+\omega_1 = \alpha_1, \qquad \zeta_2+\omega_2 = \alpha_2 \end{aligned} \tag{14}$$

The above equations constitute a system of 34 equations for 34 unknowns, the 16 member lengths (e_1, f_1, e_2, f_2, e_3, f_3, e_4, f_4, a_1, b_1, c_1, d_1, a_2, b_2, c_2, d_2), the 16 angles (ε_1, γ_1, ε_2, γ_2, ε_3, γ_3, ε_4, γ_4, α_1, θ_1, δ_1, ζ_1, α_2, θ_2, δ_2, ζ_2)

and the unit dimensions h_2, h_3. As already mentioned, the structural thickness h_1 is a known design parameter. As far as the solution of the above system is concerned, Eqs. (8a), (10a), (12a) and (14d) are linearly independent and they can be solved as a 4 by 4 system. Since all coordinates of the nodes of the first SLE ($A_1A_2B_1B_2$) are known, the lengths e_1, f_1 and the angles ε_1, γ_1 can thus be derived. Then, a system of 30 non-linear equations for 30 unknowns remains to be solved numerically.

2.2. Geometric constraints taking joint dimensions into account

The derivation of geometric constraints and formulation of geometric design procedures in the previous section was based on the assumption that the hubs are 'perfect', dimensionless hinges. In reality, however, they have some discrete dimensions, which should be taken into account during geometric design, in order to avoid geometric non-fit of the members, assembling problems, and violation of the desired stress-free state in the folded and deployed configuration. The type of circular joints with radius r, used in our experimental models, is shown in Fig. 14. It should be noted that the angles between planes of adjacent SLEs remain unchanged during the deployment process, thus the hinges only have to accommodate axial forces of the members converging into them.

In order to derive the geometric constraints with discrete joint dimensions, we consider again the development of outer (Fig. 15) and inner (Fig. 16) SLEs on a common plane. Furthermore, we consider the development of adjacent SLEs on a common plane. The geometric constraints differing from those that were derived earlier for idealized joints concern the length projections in the tangential direction:

- For the outer SLEs, Eq. (12) should be replaced by:

$$\begin{aligned} &2f_1 \sin\left(\frac{\varepsilon_1+\gamma_1}{2}\right) + 2r\cos\frac{\varphi_1}{2} = g_1, \qquad 2f_2 \sin\left(\frac{\varepsilon_2+\gamma_2}{2}\right) + 2r\cos\frac{\varphi_2}{2} = g_1 \\ &f_3\cos(\psi_1-\gamma_3) + f_4\cos(\psi_2-\gamma_4) + r(\sin\psi_1+\sin\psi_2) = g_2 \end{aligned} \tag{15}$$

- For the inner SLEs, Eq. (13) should be replaced by:

$$\begin{aligned} &b_1\cos(\psi_3-\theta_1) + c_1\cos(\psi_4-\zeta_1) + r(\sin\psi_3+\sin\psi_4) = L_1 \\ &b_2\cos(\psi_5-\theta_2) + c_2\cos(\psi_6-\zeta_2) + r(\sin\psi_5+\sin\psi_6) = L_2 \end{aligned} \tag{16}$$

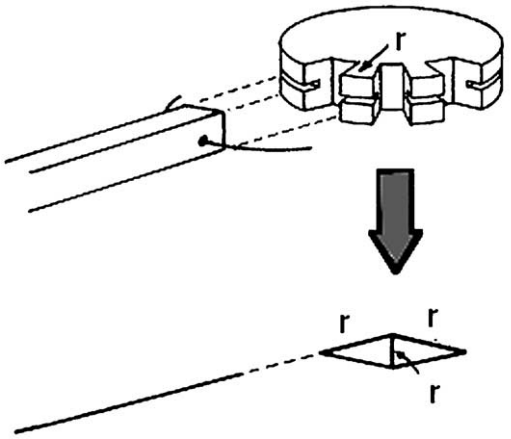

Fig. 14. Real joint and corresponding model.

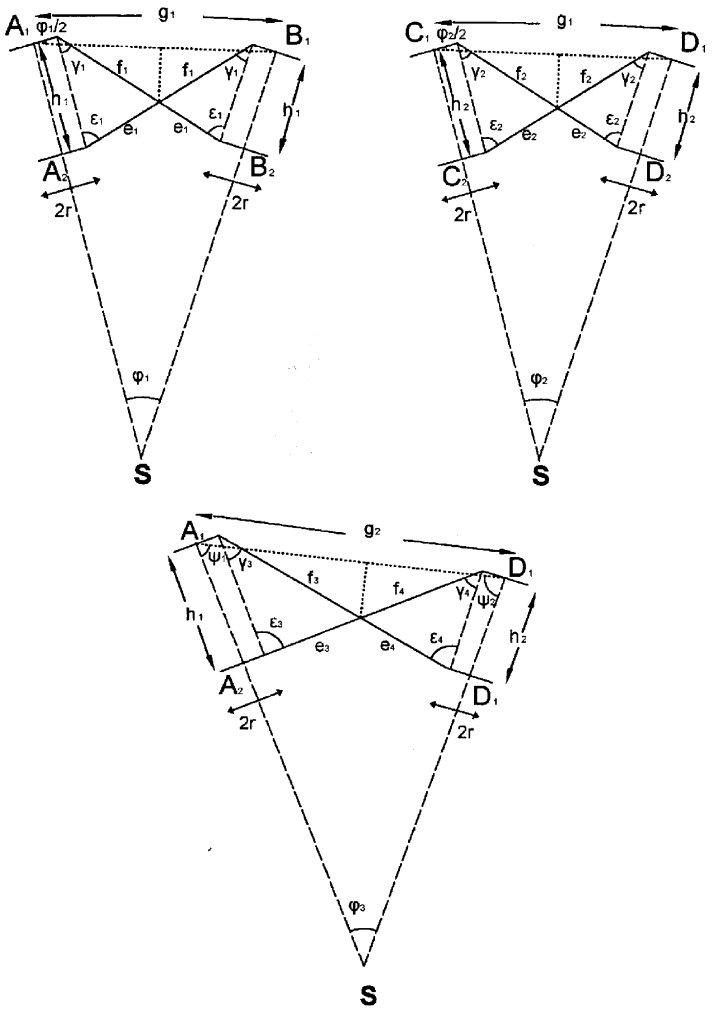

Fig. 15. Outer SLEs accounting for joint dimensions.

3. Geometric design

The detailed application of the proposed design methodology for each single unit consists of the following steps:

(i) The coordinates of A_1 and B_1 are considered as known. These points, as illustrated in Fig. 7, belong to the elliptical surface and more specifically to the edge ellipses on both sides of the axis. The x coordinate of A_1, B_1 is equal to the dimension a of the ellipse and the y coordinate is equal to zero.
(ii) The point S (0,0,0) is the center of the ellipse.
(iii) The coordinates of C_1 and D_1 are derived by the subdivision of the elliptical surface and belong to the edge ellipses.

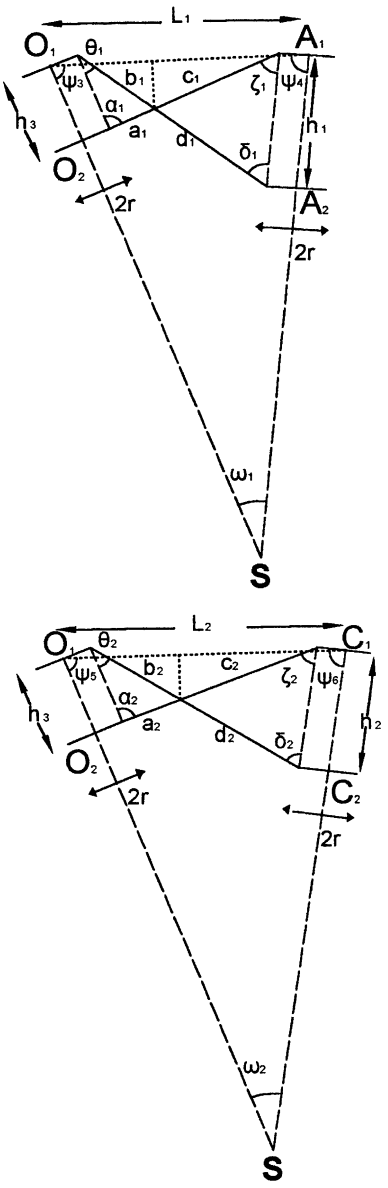

Fig. 16. Inner SLEs accounting for joint dimensions.

(iv) The point O_1 belongs to the elliptical surface and more specifically it is located in the middle of the arch of each single unit. The coordinates of O_1 are derived from the following system of two simultaneous equations:

$$\frac{x_{O1}^2}{a^2}+\frac{y_{O1}^2}{b^2}=1, \qquad y_{O1}=\tan\left(\frac{\lambda}{2}\right)\cdot x_{O1} \tag{17}$$

where $\lambda/2$ is the angle of direction of O_1 (Fig. 9).

(v) Considering all the above as known parameters, the values of lengths L_1, L_2 and angles φ_1, φ_2, φ_3, ω_1, ω_2, ψ_1, ψ_2, ψ_3, ψ_4, ψ_5, ψ_6 can be derived by equations similar to (3) and (4).

(vi) Then, the values of lengths e_1, f_1 and angles ε_1, γ_1 are derived from the linearly independent simultaneous equations (8a), (10a), (14d) and (15a).

(vii) Next, the system of 30 non-linear simultaneous equations (5a,b), (6), (7a,b), (8b–d), (9a–d), (10b–d), (11a–d), (14a–c,e–h), (15b,c), (16a,b) is solved, in order to obtain the remaining unknown lengths e_2, f_2, e_3, f_3, e_4, f_4, a_1, b_1, c_1, d_1, a_2, b_2, c_2, d_2, the angles ε_2, γ_2, ε_3, γ_3, ε_4, γ_4, α_1, θ_1, δ_1, ζ_1, α_2, θ_2, δ_2, ζ_2 and the parameters h_2, h_3.

(viii) Considering the coordinates of the upper nodes and the respective thickness of each unit as known, the coordinates of the lower nodes can then be calculated.

(ix) Finally for each point A_i, B_i, C_i and D_i the coordinates of the discrete joints $A_{i\mathrm{a}}$, $B_{i\mathrm{a}}$, $C_{i\mathrm{a}}$ and $D_{i\mathrm{a}}$, shown in Fig. 17, can be obtained by solving corresponding systems of three simultaneous equations, for example for point $A_{1\mathrm{a}}$:

$$\begin{vmatrix} x_{A1\mathrm{a}} & y_{A1\mathrm{a}} & z_{A1\mathrm{a}} & 1 \\ x_{A1} & y_{A1} & z_{A1} & 1 \\ x_{O1} & y_{O1} & z_{O1} & 1 \\ x_S & y_S & z_S & 1 \end{vmatrix} = 0$$
$$\ell_{A1}(x_{A1\mathrm{a}} - x_{A1}) + m_{A1}(y_{A1\mathrm{a}} - y_{A1}) + n_{A1}(z_{A1\mathrm{a}} - z_{A1}) = 0 \tag{18}$$
$$r = \sqrt{(x_{A1} - x_{A1\mathrm{a}})^2 + (y_{A1} - y_{A1\mathrm{a}})^2 + (z_{A1} - z_{A1\mathrm{a}})^2}$$

The first of Eqs. (18) specifies that $A_{1\mathrm{a}}$ belongs in the plane defined by points A_1, O_1 and S. Eq. (18b) indicates that $A_{1\mathrm{a}}$ belongs in the plane perpendicular to line A_1S at point A_1. The values ℓ_{A1}, m_{A1}, n_{A1} are the known cosines of direction of line A_1S. Finally, Eq. (18c) denotes that the distance between $A_{1\mathrm{a}}$ and A_1 is equal to the known radius r of the circular node.

The initial values needed for the iterative solution of the 30 simultaneous non-linear equations can be obtained by starting with the geometric design of a semi-circular arch ($a = b$), and then reducing radius b gradually and using the solutions of the previous step as trial values for the next step.

4. Application

The above process has been applied for the geometric design of the semi-elliptical arch shown in Fig. 18, with a span of 13.622 m, a height of 6.130 m and a structural thickness of 0.811 m at the two supports. The main objective of this exercise was to confirm the correctness of the geometric constraint equations and the proposed geometric design approach, and to verify the deployability potential of a deployable arch with varying curvature. Design of an optimized real structure, able to withstand realistic loads was not sought at this stage, thus several simplifying assumptions have been adopted. Hence, finite element analysis of the deployed arch under service loads was only performed for reasons of completeness and in order to show that the resulting deflections and member forces are of an order of magnitude acceptable for real applications. Structural optimization in order to achieve a better balance between the response during deployment and under service loads will be carried out in future work. The deployability feature of the arch has been verified both by constructing a small-scale physical model and by finite element analysis. This example is presented in detail next.

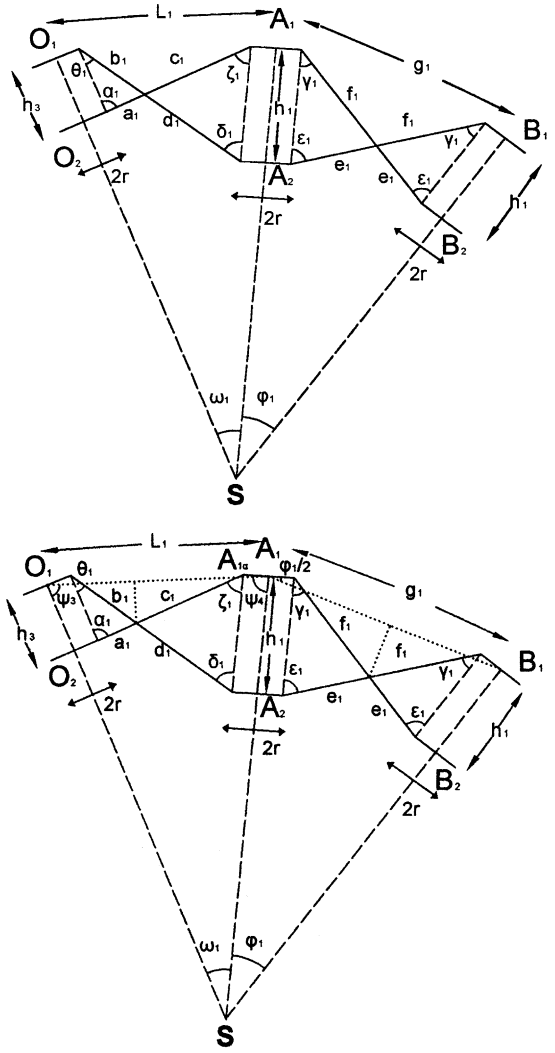

Fig. 17. Adjacent outer and inner SLEs accounting for joint dimensions.

4.1. Geometric design

Assuming that the radii a, b of the ellipse are known ($a = 6.811$ m, $b = 0.90 * 6.811 = 6.130$ m), the length of the semi-elliptical arch is found equal to 20.3418 m. The arch is divided into eight segments with the same length, 2.54272 m. The length of each respective chord is different and more specifically equal to 2.52103, 2.52479, 2.52855 and 2.53049 m for the first, second, third and fourth unit, respectively. This value is the g_2-parameter for each unit. The g_1-parameter is common for all units and equal to the average of the four g_2 ($g_1 = 2.52621$ m).

In order to obtain initial values for the numerical iterative solution of the geometric constraint equations, the geometric design of a semi-circular arch is performed first. The arch consists of eight units and the values of radius and structural thickness are $R = 6.811$ m and $h_1 = 0.811$ m, respectively. Then, the radius b of the ellipse is gradually reduced in steps of 2% up to 10%, in comparison with the radius a. The geometric

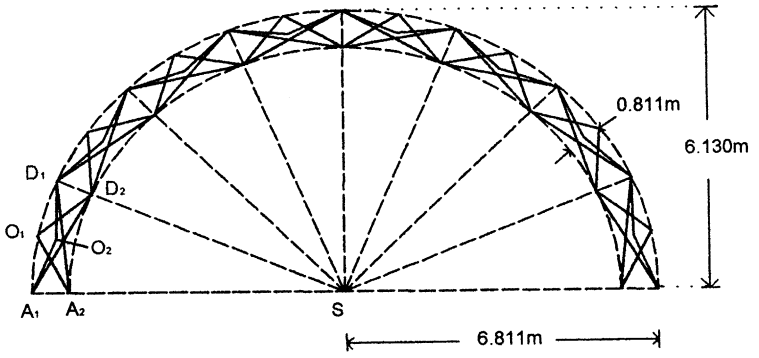

Fig. 18. Semi-elliptical arch.

quantities of each step are used as initial values for the iterations of the next step. Considering also a hub radius $r = 0.12$ m, the geometric design of the desired arch of semi-elliptical shape is achieved. The pertinent geometric quantities of the four units are listed in Table 1.

4.2. Physical model

The geometric design methodology has been verified through the construction of a physical model in scale 1:20, shown in Fig. 19 in some successive deployment stages. The members of the arch are made of straws, the outer hubs of circular wire rings and the pivotal connections of metal pins. One very interesting issue arising for the deployment of such structures, namely how the difference in geometry between adjacent units affects the way and the sequence in which the individual units undergo snap-through and how they interact during that process, can be qualitatively observed by means of this model. "Flatter" units, characterized by b_1/a_1 and b_2/a_2 ratios close to 1, are softer and tend to buckle first. This issue will be further explored in future work, and will be utilized to control better the deployment intensity, and to optimize the overall design.

4.3. Material and cross-section characteristics

The selection of suitable materials and cross-sections for the members must be such that several design objectives are met. Namely, the stiffness of the deployed arch under service loads must be satisfactory, with specific deflection limits depending on the intended use. This can be achieved by providing sufficient intensity of snap-through during deployment, but without requiring too much energy or allowing material non-linearities. At the same time, a lightweight material improves handling and transportation.

In order to satisfy all the above requirements, several iterations were needed. They resulted in choosing low-density polyethylene (Young's modulus $E = 150$ MPa, yield stress $\sigma_y = 20$ MPa) for the outer SLEs, and acrylic ($E = 80$ MPa, $\sigma_y = 15$ MPa) for the inner SLEs. The hubs are made also of low-density polyethylene. As far as the cross-sections of the members are concerned, the outer SLEs use a rectangular hollow section of 150 mm by 60 mm with a 15 mm wall thickness and the inner SLEs, which are mainly responsible for controlling the snap-through intensity, a rectangular hollow section of 110 mm by 50 mm with a 15 mm wall thickness (Fig. 20).

Based on the above selections of materials and cross-sections, the deployability of the structural unit was feasible, but the response of the structure under some service load combinations was not satisfactory due to large deflections under vertical loads. This was solved by placing connection rods between the upper and

Table 1
Geometric quantities of the prototype arch

		First unit	Second unit	Third unit	Fourth unit
g_1	m	2.52621			
g_2		2.52103	2.52479	2.52855	2.53049
λ	rad	0.374887	0.38409	0.399579	0.41224
φ_1		0.366736	0.372327	0.386089	0.40034
φ_2		0.372327	0.386089	0.40034	0.406418
φ_3		0.368443	0.377185	0.391844	0.403778
ω_1		0.261464	0.266665	0.276918	0.286327
ω_2		0.263409	0.271454	0.281865	0.288429
ψ_1		1.34646	1.28854	1.28499	1.33261
ψ_2		1.42669	1.47586	1.46476	1.4052
ψ_3		1.51961	1.566	1.57154	1.537
ψ_4		1.36052	1.30893	1.29314	1.31826
ψ_5		1.46175	1.43073	1.44141	1.48434
ψ_6		1.41643	1.43941	1.41832	1.36882
L_1	m	1.79298	1.79833	1.79999	1.79517
L_2		1.78748	1.78282	1.78183	1.78696
h_1		0.811	0.816955	0.795216	0.769353
h_2		0.816955	0.795216	0.769353	0.756161
h_3		0.307553	0.336339	0.330884	0.265407
e_1		1.06408	1.06167	1.05685	1.05244
f_1		1.22187	1.22318	1.21925	1.21465
e_2		1.06167	1.05685	1.05246	1.05074
f_2		1.22318	1.21925	1.21464	1.21227
e_3		1.0726	1.03506	1.0249	1.03953
f_3		1.21335	1.24978	1.2512	1.22756
e_4		1.05359	1.08391	1.08449	1.06183
f_4		1.23125	1.19218	1.1826	1.20118
a_1		0.403431	0.41756	0.420026	0.408255
b_1		0.456396	0.499245	0.502075	0.406734
c_1		1.18608	1.15897	1.15589	1.25091
d_1		1.09986	1.12588	1.12021	1.01618
a_2		0.408081	0.403212	0.403327	0.400925
b_2		0.451747	0.513592	0.518775	0.414064
c_2		1.19916	1.12059	1.11178	1.22747
d_2		1.08568	1.1555	1.15531	1.03554
ε_1	rad	1.39784	1.39792	1.41385	1.43193
γ_1		1.03111	1.02559	1.02776	1.03159
ε_2		1.39792	1.41385	1.43193	1.4406
γ_2		1.02559	1.02776	1.03159	1.03418
ε_3		1.37647	1.46606	1.49799	1.46648
γ_3		1.04986	0.967822	0.955948	1.00197
ε_4		1.41831	1.34501	1.34779	1.40575
γ_4		1.00802	1.08888	1.10615	1.0627
α_1		1.37184	1.43425	1.44897	1.23639
θ_1		1.04817	0.976598	0.97929	1.24155
δ_1		1.30963	1.24326	1.25621	1.52788
ζ_1		1.11037	1.16758	1.17205	0.950064
α_2		1.34154	1.52681	1.55949	1.28981
θ_2		1.07524	0.901606	0.890084	1.18676
δ_2		1.33865	1.17306	1.17195	1.47519
ζ_2		1.07813	1.25535	1.27762	1.00139

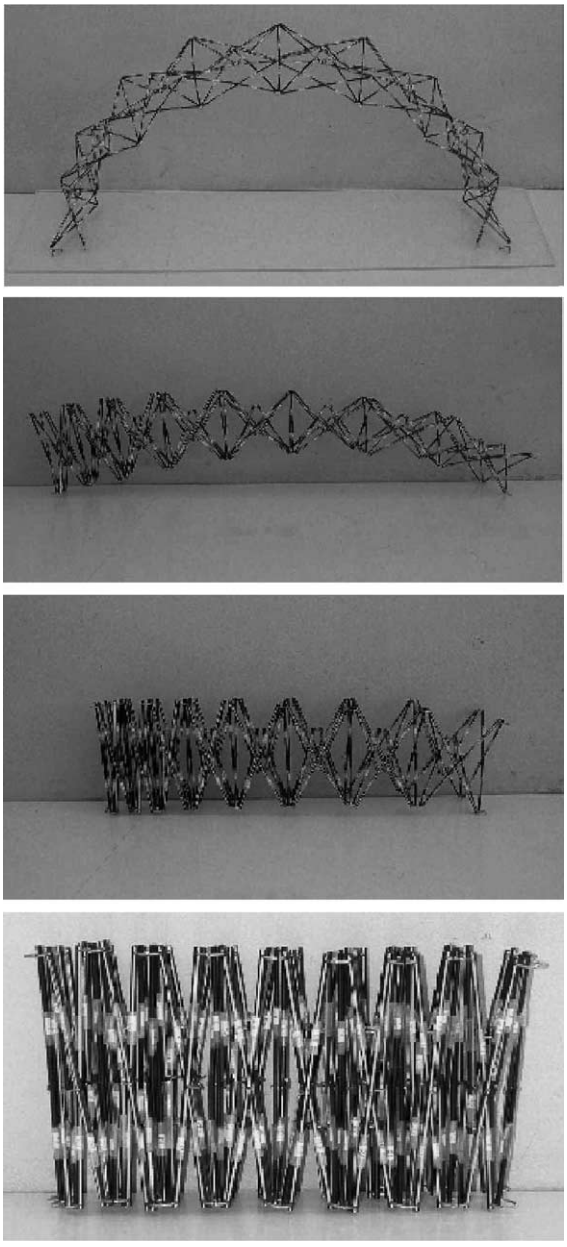

Fig. 19. Successive deployment stages of the physical model.

the lower nodes of each unit (Fig. 21a), thus enhancing the stiffness of the deployed structure. This intervention violates the design target of having exactly the same structural system for the folded and the deployed structure (with the exception of different boundary conditions), and increases slightly the time and effort required for deployment and disassembling. But the intervention related to the placement of the connection rods is considered minimal and is still a good compromise between ease of deployment and desired structural characteristics.

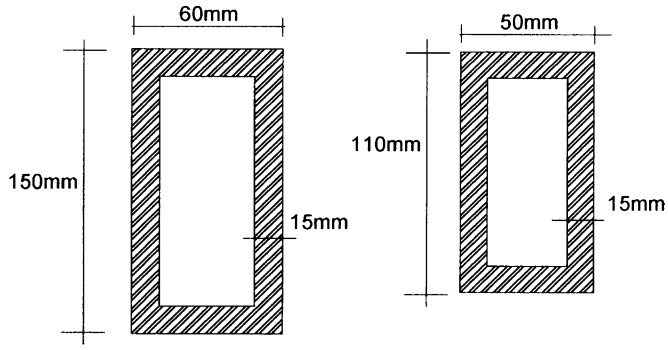

Fig. 20. Cross-sections of the outer and inner SLEs.

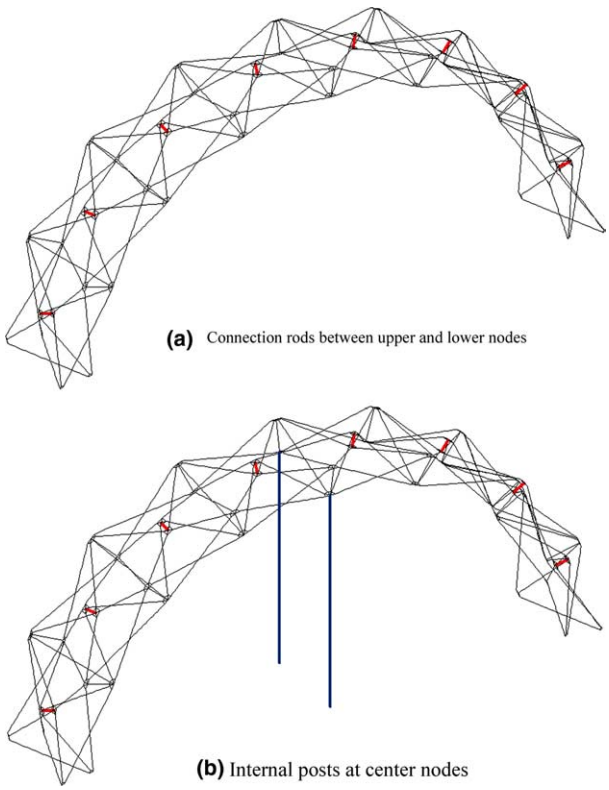

Fig. 21. Means to increase stiffness of the deployed arch.

In cases of maximum snow load there were further violations of the serviceability limits (deflections smaller than span length over 250), that can be prevented by supporting (for example by means of vertical posts) the two lower nodes at the center of the arch (Fig. 21b), thus reducing deflections by 50%. This will be needed only if the structure is to be used in climates justifying such loads, and only during the rare events when such loads will be indeed realized. Even then, only serviceability and not strength will be violated if

the supporting posts are not put into place. Thus, the undesirable presence of the posts in the interior of the structure will be needed only in very few cases.

Hence, it is considered that the structure demonstrated a satisfactory behavior during both stages of analysis that will be described next.

4.4. Finite element analysis

For the analysis the finite element program MSC/NASTRAN 4.0 for Windows was used. The members of inner and outer SLEs were modeled with beam elements, and the hubs were modeled as equivalent grids of beam elements. The static analysis of the structure consisted of two stages:

(i) *Linear analysis of the arch in the deployed configuration, in order to obtain displacements and stresses under service loads.*

For this analysis the arch was considered pinned at both ends. The loads that were taken into account for the linear analysis are the dead weight of the structure, snow with 0.3 m thickness and a 0.5 kN/m^2 wind pressure, using tributary areas to distribute them on the individual arch members. Indicative results of deformation (maximum total translation 23.5 mm) and axial forces in the members (maximum tension 13.69 N, maximum compression 14.09 N) are shown in distorted scale in Fig. 22 for the case of simultaneous action of dead, snow and wind loads. The maximum stresses are well below the yield stresses of the respective materials, while the maximum deflections under dead loads are marginally within the service-

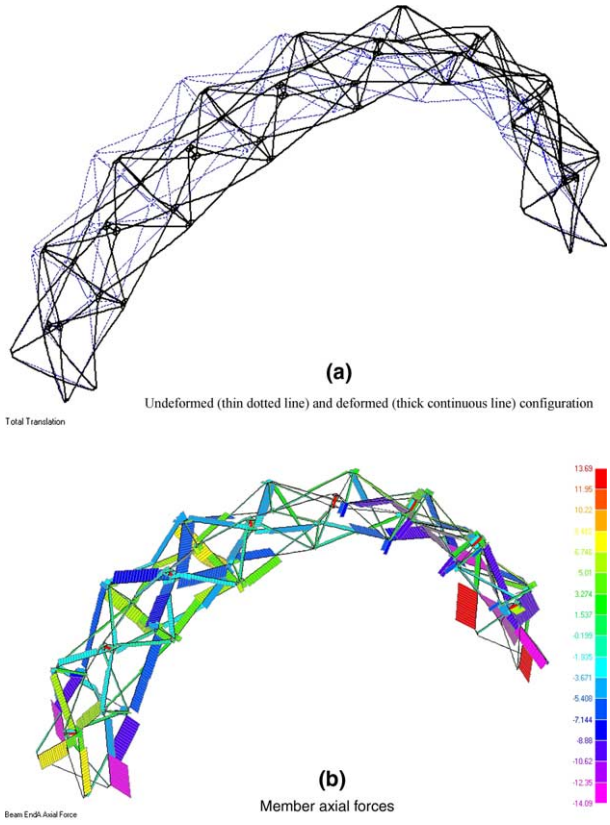

Fig. 22. Deformation and axial forces for load combination (dead + snow + wind).

ability limits of span length over 250 without vertical posts, but require the posts in order to satisfy serviceability for snow and wind loads.

(ii) *Non-linear analysis of each single structural unit, in order to verify deployability and to compute stresses during deployment as well as the required deployment load.*

Taking advantage of the fact that deployability of the whole arch was verified by means of the physical model, numerical deployment simulation was carried out for each individual unit separately, as deployment stresses are deformation-induced and can be predicted very accurately in this manner (Gantes, 2001). During this process the members are subjected to axial forces and bending moments and, thus, they develop normal longitudinal stresses. The lower center node of the unit was assumed as pinned and a controlled

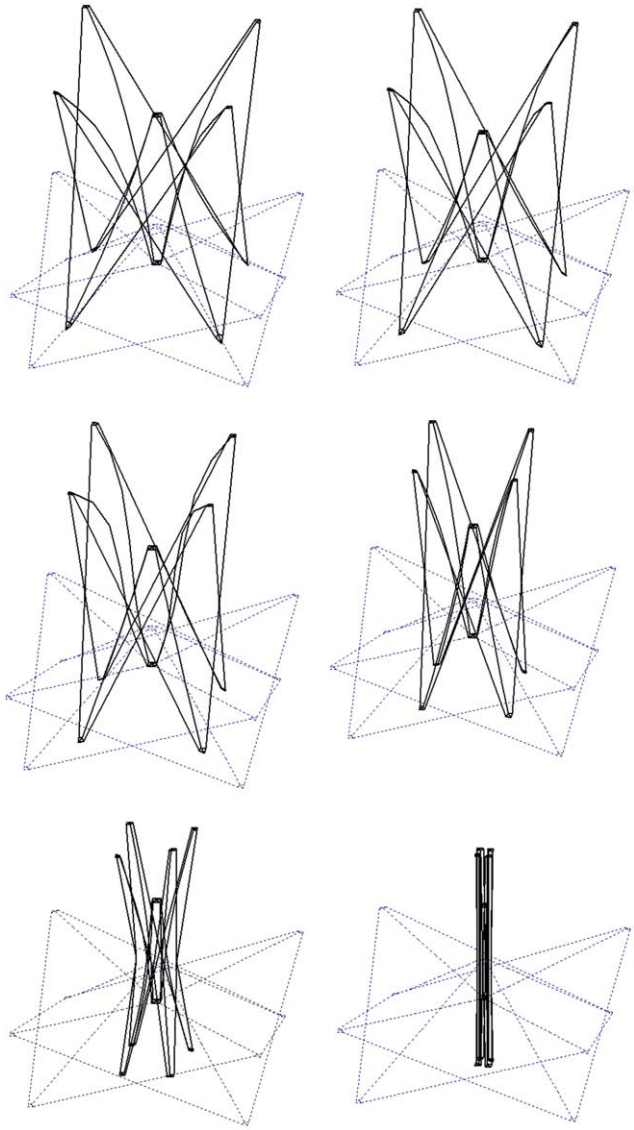

Fig. 23. Successive deformed configurations as obtained from finite element simulation of dismantling.

displacement was imposed on the upper center node, in the direction defined by the upper and lower center nodes. All other nodes were free except for prevention of rigid body rotation. Full Newton–Raphson iterations were carried out in 60 steps with 150 maximum iterations per step. Dismantling was simulated instead of deployment due to improved performance of the non-linear iterative algorithm.

Fig. 23 shows successive dismantling stages as obtained from the above analysis. The deformed configuration is shown with thick continuous line and the undeformed one with thin dotted line. Fig. 24 illustrates the corresponding non-linear load–displacement path. The quantity δ in the horizontal axis is the relative vertical displacement between upper and lower center nodes, while the load P in the vertical axis is the external load required for deployment, obtained as the reaction corresponding to the imposed displacement. The snap-through nature of the response is clearly indicated.

The maximum value of the required deployment load, obtained from numerical analysis as equal to approximately 5 kN, indicates the need for mechanical equipment in order to realize deployment. This is justified, taking into account the size of the structure and the significant service loads employed for analysis in the deployed configuration, however, a more favorable selection of materials, member cross-sections and required deployment loads is expected to be possible by means of structural optimization (Gantes, 2000a,b).

The maximum stresses that develop in the members of inner SLEs during deployment are approximately equal to 10.5 MPa, which is 70% of the yield stresses of 15 MPa. The outer SLEs are not stressed significantly during deployment, as expected also from previous experience with this type of structures (Gantes, 2001). Thus, the design criterion—that the material remains within the elastic range during deployment—is satisfied.

An interpretation of Fig. 24 can also lead to a better understanding of the bi-stable nature of deployable structures of this type. The geometric incompatibilities between member lengths during the deployment process leads to a highly non-linear behavior and ultimately to snap-through. The strain energy stored in

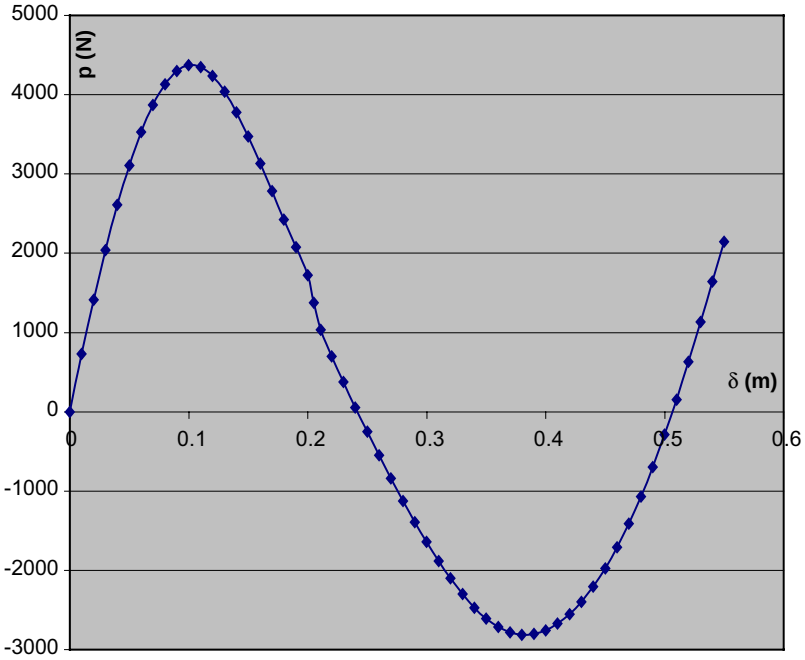

Fig. 24. Load–displacement path as obtained from finite element simulation of dismantling.

the members prior to snap-through and released afterwards, acts as a form of prestressing and locks the structure in its deployed configuration. Its stiffness is further enhanced by employing in the deployed configuration different boundary conditions from those during deployment (and in some cases additional members as well), so that unlocking is prevented under service loads. Dismantling is possible by removing the additional boundary conditions (and the additional members) and applying opposite loads to those needed for deployment. Thus, two distinct, stable phases exist, the folded and the deployed one, each characterized by different geometry, loading and boundary conditions.

5. Summary and conclusions

Deployable structures that are self-standing and stress-free when fully closed or fully deployed but exhibit incompatibilities between the member lengths at intermediate geometric configurations during the deployment process, which lead to second-order strains and stresses and a snap-through phenomenon that "locks" the structures in their deployed configuration have been investigated. A geometric design methodology for deployable arches of arbitrary curvature, accounting also for the discrete joint size, has been proposed, thus overcoming a previous disadvantage of such structures that could be only flat or curved with constant curvature. The methodology has been applied successfully for the geometric design of a semi-elliptical arch. Verification of deployability has been achieved by the construction of a small-scale physical model as well as by deployment simulation with the finite element method. A preliminary structural design indicates the overall feasibility of such an arch with a span of 13.6 m, subjected to dead, snow and wind loads.

Acknowledgements

The authors would like to thank the two anonymous reviewers for some very insightful comments that significantly helped improve the quality of this article.

References

Escrig, F.P., Brebbia, C.A., 2000. Third International Conference MARAS 2000 Mobile and Rapidly Assembled Structures, Madrid, Spain.

Escrig, F., Valcarcel, J.P., Gil Delgado, O., 1989. Design of expandable spherical grids. In: Proceedings of the XXX IASS Congress, Madrid, Spain.

Furuya, H., Kawasaki, Y., 2000. Effects of folding parameters on surface accuracy of deployable membrane space structures. In: Proceedings of the 41st AIAA/ASME/ASCE/AHS/ASC Structures, Structural Dynamics and Material Conference, Inflatable Structures Forum, AIAA-2000-1731, Atlanta, pp. 1–7.

Gantes, C., 1991. A design methodology for deployable structures. Ph.D. Thesis, available as Research Report No. R91-11, Department of Civil Engineering, MIT, Cambridge, Massachusetts.

Gantes, C., 1993. Geometric constraints in assembling polygonal deployable units to form multi-unit structural systems. In: Parke, G.A.R., Howard, C.M. (Eds.), Proceedings of the Fourth International Conference on Space Structures, Surrey, United Kingdom, Thomas Telford, London, pp. 793–803.

Gantes, C., 1996. A creative aspect of a destructive phenomenon: using snap-through buckling as a form of prestressing. In: Proceedings of IASS/IABSE International Symposium on Conceptual Design of Structures, Stuttgart, Germany, vol. I, pp. 222–229.

Gantes, C.J., 1997. An improved analytical model for the prediction of the nonlinear behavior of flat and curved deployable space frames. Journal of Constructional Steel Research 44 (1–2), 129–158.

Gantes, C.J., 2000. Nonlinear structural behavior, analysis and design of deployable structures. In: Proceedings of NATO Advanced Research Workshop on Computational Aspects of Nonlinear Structural Systems with Large Rigid Body Motion, Pultusk, Poland.

Gantes, C.J., 2000b. Design strategies for controlling structural instabilities. International Journal of Space Structures 15 (3 & 4), 167–188.

Gantes, C.J., 2001. Deployable Structures—Analysis and Design. WIT Press, Southampton, England.

Gantes, C.J., Konitopoulou, E., 2002. Snap-through-type deployable structures with arbitrary curvature. In: Proceedings of the 5th International Conference on Space Structures, Surrey, UK.

Gantes, C., Connor, J.J., Logcher, R.D., 1991. Combining numerical analysis and engineering judgement to design deployable structures. Computers & Structures 40 (2), 431–440.

Gantes, C., Connor, J.J., Logcher, R.D., 1993a. Simulation of the deployment process of multi-unit deployable structures on a Cray-2. International Journal of Supercomputer Applications 7 (2), 144–154.

Gantes, C., Connor, J.J., Logcher, R.D., 1993b. A simple friction model for scissor-type mobile structures. Journal of Engineering Mechanics, ASCE 119 (3), 456–475.

Gantes, C., Logcher, R.D., Connor, J.J., Rosenfeld, Y., 1993c. Deployability conditions for curved and flat, polygonal and trapezoidal deployable structures. International Journal of Space Structures 8 (1/2), 97–106.

Gantes, C., Logcher, R.D., Connor, J.J., Rosenfeld, Y., 1993d. Geometric design of deployable structures with discrete joint size. International Journal of Space Structures 8 (1/2), 107–117.

Gantes, C., Connor, J.J., Logcher, R.D., 1994a. A systematic design methodology for deployable structures. International Journal of Space Structures 9 (2), 67–86.

Gantes, C., Connor, J.J., Logcher, R.D., 1994b. Equivalent continuum model for deployable flat lattice structures. Journal of Aerospace Engineering, ASCE 7 (1), 72–91.

Gantes, C., Giakoumakis, A., Vousvounis, P., 1997. Symbolic manipulation as a tool for design of deployable domes. Computers & Structures 64 (1–4), 865–878.

Kawaguchi, K., Kondo, S., 2000. A deployable frame for single layer lattice frames. In: Kwun, T.J., Lee, D.G. (Eds.), Proceedings of the 6th Asian Pacific Conference on Shell and Spatial Structures, vol. I. Hakmun Pub. Inc., pp. 175–182.

Konitopoulou, E., 2001. Geometric design of deployable arches with arbitrary curvature and their structural analysis using the finite element method. Diploma Thesis, Civil Engineering Department, National Technical University of Athens (in Greek).

Krishnapillai, S., Zalewski, W.P., 1985. The design of deployable structures. Unpublished Research Report, Department of Architecture, MIT, Cambridge, Massachusetts.

Kuznetsov, E.N., 1991. Underconstrained Structural Systems. Springer Verlag, New York.

Kwan, A.S.K., Pellegrino, S., 1991. The pantographic deployable mast: design, structural performance, and deployment tests. In: Proceedings of: MARAS'91, International Conference on Mobile and Rapidly Assembled Structures, Southampton, UK, pp. 213–224.

Langbecker, T., Albermani, F., 2001. Kinematic and nonlinear analysis of foldable barrel vaults. Engineering Structures 23 (2), 158–171.

Merchan, C.H.H., 1987. Deployable structures. S.M. Thesis, MIT Architecture Department.

Miura, K., Furuya, H., 1988. Adaptive structure concept for future space applications. AIAA Journal 26 (8), 995–1002.

Pellegrino, S., Guest, S.D., 2000. IUTAM-IASS Symposium on Deployable Structures: Theory and Applications. Kluwer Academic Publishers, Dordrecht.

Pinero, E.P., 1962. Expandable space framing. Progressive Architecture 43 (6), 154–155.

Rhodes, M.D., 1984. New concepts in deployable beam structures. In: NASA Conference Publication 2368, Part 1, Large Space Antenna Systems Technology Conference, Hampton, Virginia, pp. 331–348.

You, Z., 2000. Deployable structure of curved profile for space antennas. ASCE Journal of Aerospace Engineering 13 (4), 139–143.

You, Z., Pellegrino, S., 1993. Foldable ring structures. In: Parke, G.A.R., Howard, C.M. (Eds.), Proceedings of Fourth International Conference on Space Structures, Thomas Telford, Surrey, United Kingdom.

Zeigler, T.R., 1984. Collapsable self-supporting structures. US Patent No. 4,437,275.